

Entropic wetting of a colloidal rod-sphere mixture

R. ROTH^{1,2}, J. M. BRADER³ and M. SCHMIDT⁴(*)

¹ *Max-Planck-Institut für Metallforschung - Heisenbergstr. 3, 70569 Stuttgart, Germany*

² *ITAP, Universität Stuttgart - Pfaffenwaldring 57, 70569 Stuttgart, Germany*

³ *Institute of Physiology, University of Bern - Bühlpplatz 5, 3012 Bern, Switzerland*

⁴ *Soft Condensed Matter, Debye Institute, Utrecht University*

Princetonpln 5, 3584 CC Utrecht, The Netherlands

(received 28 March 2003; accepted in final form 16 June 2003)

PACS. 68.08.Bc – Wetting.

PACS. 82.70.Dd – Colloids.

PACS. 64.70.Ja – Liquid-liquid transitions.

Abstract. – We investigate the behavior of a model colloidal mixture of hard spheres and rod-like particles near a planar hard wall using density functional theory. For small size ratios of rod length and sphere diameter we find that the colloidal liquid phase wets the wall completely upon approaching the fluid demixing binodal from the colloidal gas side, provided the density of the rods lies below the wetting point. Using an effective one-component description based on the pairwise depletion potential for higher density of rods, a finite sequence of layering phase transitions is found. For large rod-to-sphere size ratios, using a binary treatment, thick films are obtained even close to the triple point.

Purely repulsive interactions between the constituent mesoscopic particles may lead to surprisingly rich bulk phase behavior of multi-component colloidal suspensions. Such systems are often viewed as a primary system of colloids with added “depletant agents” that mediate an effective interaction between the particles of the primary component. Adding depletant agents to a colloidal hard-sphere dispersion may, under appropriate conditions, drive a fluid-fluid demixing phase transition, which is reminiscent of the gas-liquid transition in atomic and molecular fluids: The phase that is poor in colloids (and rich in depletants) corresponds to the gas and the phase that is rich in colloids (and poor in depletants) corresponds to the liquid phase. Among the broad range of depletant agents notable examples are smaller-sized spheres and globular non-adsorbing polymers. Another case of intriguing depletants are elongated particles, like colloidal rods or stretched polymers. One reason for such depletants being very interesting is the possibility of liquid-crystalline order, which will further enrich the bulk phase behavior [1] and the correlations between spheres [2].

For conditions where the density of rods is well below the onset of nematic order, much work has been devoted to understanding the bulk phase behavior of rod-sphere mixtures [3–8]. Among the different techniques employed are computer simulations [3], free-volume [3,4] and liquid integral equation [5] theories, as well as experiments with silica spheres mixed with silica-coated bohemite rods [4,6] or (semi-flexible) polymeric rods [7,8]. It can be concluded

(*) On leave from Institut für Theoretische Physik II, Heinrich-Heine-Universität Düsseldorf - Universitätsstraße 1, D-40225 Düsseldorf, Germany.

that the gas, fluid, and solid phase are thermodynamically stable and that the density of rods (often one uses the density in a hypothetical reservoir of rods) plays a role similar to that of inverse temperature in simple fluids. The second control parameter is the ratio of rod length L and sphere diameter σ ; for large enough values stable bulk fluid-fluid demixing occurs.

One approach to describe such complex systems is based on the depletion picture where the depletants are regarded as mediating an effective interaction between the spheres [9–13]. Theoretically, one integrates out the depletant degrees of freedom in the partition sum [9, 13] to obtain the effective interactions, which have, in general, a many-body character. Under suitable conditions one may take into account only the one- and two-body contributions. Experimentally, one can measure the forces directly, *e.g.*, between two spheres [10] or between a sphere and a wall [12] immersed in a sea of rods.

Despite the considerable interest in the bulk properties of rod-sphere mixtures little is known about their behavior at interfaces. This is in contrast to the case of mixtures of colloidal spheres and globular non-adsorbing polymer, where recent results [14–16] indicate surprisingly rich behavior at a simple hard wall. Theoretical predictions of wetting and layering surface phase transitions [14] have been validated by computer simulations [15] and, partly, experimentally [16, 17], in particular by light microscopy in a mixture of silica spheres and poly(dimethyl siloxane) dispersed in cyclohexane [16]. The emerging picture is that the colloidal liquid wets the wall completely for sufficiently low polymer concentrations (on the gas-branch of the gas-liquid binodal). For higher polymer concentrations, partial wetting occurs via an unusual (finite) sequence of layering transitions, which has been attributed to the presence of many-body effective depletion interactions between the colloidal spheres [14, 15]. The layering behavior has not yet been experimentally confirmed.

In this letter we report on density functional [18] results for the interface behavior of a model rod-sphere mixture exposed to a hard wall. For equally sized species we find that the colloidal liquid wets the wall completely upon approaching the gas branch of the demixing binodal for low rod densities. There occurs a first-order wetting transition to the partial-wetting regime for higher rod densities. In the partial-wetting regime we can identify a finite number of distinct lines where a jump in the adsorption occurs. These results are obtained by a treatment that only includes the pair-wise contribution to the depletion interaction, and hence questions the above conjecture that many-body terms are a prerequisite for the occurrence of a finite sequence of layering transitions in the partial-wetting regime. We test the robustness of these results: Complete wetting remains upon including all higher body interactions, *i.e.* treating the full mixture. For longer rod-sphere size ratios, thick films result even for high rod densities, *i.e.* close to the triple point.

We use a model proposed in [3] and employed by others [5, 9, 13, 19, 20] that can be viewed as the most simplistic binary mixture that still captures the essentials: Hard spheres (species S) of diameter σ are mixed with hard needle-like rods (species N) of length L and vanishing thickness. The one-body density distributions are denoted by $\rho_S(\mathbf{r})$ and $\rho_N(\mathbf{r}, \hat{\omega})$, where \mathbf{r} is the space coordinate and the unit vector $\hat{\omega}$ is the (rod) orientation. This mixture is exposed to a planar smooth hard wall described by external hard-core potentials, $V_{\text{ext}}^S(\mathbf{r})$ and $V_{\text{ext}}^N(\mathbf{r}, \hat{\omega})$. Due to the symmetries of fluid states the only two relevant variables are the component of \mathbf{r} perpendicular to the wall, z , and the angle between $\hat{\omega}$ and the surface normal.

In the following a brief overview of the theory is given. In the *binary treatment* the grand potential is expressed as a functional of the density fields of both species,

$$\begin{aligned} \Omega_{\text{bin}}[\rho_S, \rho_N] = & F_{\text{id}}[\rho_S] + F_{\text{id}}[\rho_N] + F_{\text{exc}}^{\text{hs}}[\rho_S] + F_{\text{exc}}^{\text{SN}}[\rho_S, \rho_N] + \\ & + \int d\mathbf{r} \rho_S(\mathbf{r}) \left(V_{\text{ext}}^S(\mathbf{r}) - \mu_S \right) + \int d\mathbf{r} d\hat{\omega} \rho_N(\mathbf{r}, \hat{\omega}) \left(V_{\text{ext}}^N(\mathbf{r}, \hat{\omega}) - \mu_N \right), \quad (1) \end{aligned}$$

where the ideal-gas contribution is for spheres $F_{\text{id}}[\rho_S] = kT \int d\mathbf{r} \rho_S(\mathbf{r})(\ln(\rho_S(\mathbf{r})\Lambda_S^3) - 1)$ and for rods $F_{\text{id}}[\rho_N] = kT \int d\mathbf{r} d\hat{\omega} \rho_N(\mathbf{r}, \hat{\omega})(\ln(\rho_N(\mathbf{r}, \hat{\omega})\Lambda_N^3) - 1)$, where k is Boltzmann's constant, T is temperature, and Λ_i is the thermal wavelength of species $i = S, N$. The excess (over ideal gas) parts are Rosenfeld's functional [21] for hard spheres, $F_{\text{exc}}^{\text{hs}}[\rho_S]$, and the rod-sphere contribution, $F_{\text{exc}}^{\text{SN}}[\rho_S, \rho_N]$, of refs. [19, 20]. Clearly, the minimization of the grand potential needs to be performed with respect to both species, *i.e.* we solve simultaneously $\delta\Omega_{\text{bin}}/\delta\rho_S(\mathbf{r}) = 0$ and $\delta\Omega_{\text{bin}}/\delta\rho_N(\mathbf{r}, \hat{\omega}) = 0$. For practical reasons the angle between $\hat{\omega}$ and the surface normal of the wall is discretized in 60 steps, hence the latter condition is in fact a set of equations indexed by $\hat{\omega}$, see [20] for further details about the numerical strategy. This treatment takes into account all effective many-body terms, but is computationally demanding.

In the *effective one-component description* depletion potentials between spheres, W_{SS} , and between a sphere and the wall, W_{SW} , are obtained by integrating out the rod degrees of freedom [13]. Then the grand potential depends only on the sphere density distribution,

$$\begin{aligned} \Omega_{\text{eff}}[\rho_S] = & F_{\text{id}}[\rho_S] + F_{\text{exc}}^{\text{hs}}[\rho_S] + \frac{1}{2} \int d\mathbf{r} d\mathbf{r}' \rho_S(\mathbf{r}) K(|\mathbf{r} - \mathbf{r}'|) \rho_S(\mathbf{r}') + \\ & + \int d\mathbf{r} \rho_S(\mathbf{r}) \left(V_{\text{ext}}^{\text{S}}(\mathbf{r}) + W_{\text{SW}}(\mathbf{r}) - \mu_S \right), \end{aligned} \quad (2)$$

where the depletion attraction is treated in a mean-field-like manner [22]: The convolution kernel is $K(r) = W_{\text{SS}}(r)$ for $r \geq \sigma$, and $K(r) = W_{\text{SS}}(\sigma^+)$ for $r < \sigma$. Note that this is a particularly clean application of the framework: No mapping of a soft repulsion onto a hard-sphere reference system is to be performed; σ is the true physical particle size and $W_{\text{SS}}(\sigma^+)$ is the minimal value of the pair potential. The particular choice of $K(r < \sigma)$ to treat attractive interactions has been empirically found to improve the agreement between DFT and other theories. Due to the rod ideality, the depletion potentials W_{SW} and W_{SN} depend linearly on ρ_N^r , which is the density in an (ideal) reservoir of needles that is in chemical equilibrium with the system. ρ_N^r thus plays a role analogous to that of inverse temperature in simple fluids. Due to the particle geometries higher than two-body contributions vanish only for size ratios $L/\sigma < 1 - (2\sqrt{3} - 3)^{1/2} = 0.31875$. The crucial benefit of the one-component approach is that one has to deal with only one single minimization condition: $\delta\Omega_{\text{eff}}/\delta\rho_S(\mathbf{r}) = 0$.

From either approach the bulk free energy for fluid states is obtained by assuming the density field(s) to be constant. As thermodynamic variables we use the sphere packing fraction $\eta = \pi\rho_S\sigma^3/6$ and a scaled rod reservoir density, $\rho_N^r L^2\sigma$. The conditions of equal pressure and chemical potentials of both species yield the phase diagram as a function of η and ρ_N^r , as displayed in fig. 1 for $L/\sigma = 1$, which is large enough (> 0.3) so that a liquid phase exists [3]. For ρ_N^r above the critical point, phase separation occurs into a gas phase that is dilute in spheres and a liquid phase that is dense in spheres; phase coexistence is along horizontal tie lines at constant ρ_N^r . The free energy obtained from the binary treatment [19] is the same as that of [3], and was shown to give good account of the simulated coexistence curve [3]. The binodal from the effective treatment has the same qualitative behavior, the critical point, and accordingly the whole binodal, being shifted slightly toward lower densities. Comparing structure at two statepoints in the mixed region away from coexistence yields a further comparison of the consistency of both approaches; see fig. 2 for results for $\rho_S(z)$ at a hard wall. As a reference, corresponding profiles for the pure hard-sphere case (for the same values of η) are displayed. Clearly, the addition of rods leads to a strong increase near contact with the wall, $0.5 < z/\sigma < 0.7$, as well as an increase in the contact value, $\rho_S(\sigma^+/2)$, itself—the manifestation of the depletion effect. Remarkably, the results from both approaches are identical on the scale of the plot, except for a slightly higher contact value of the one-

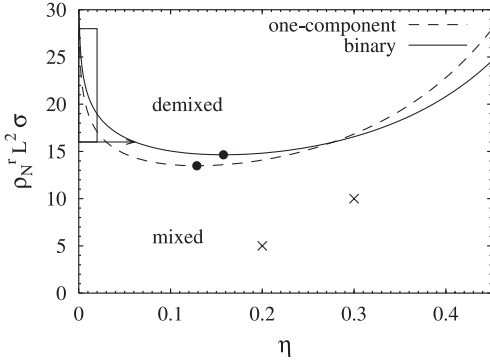


Fig. 1

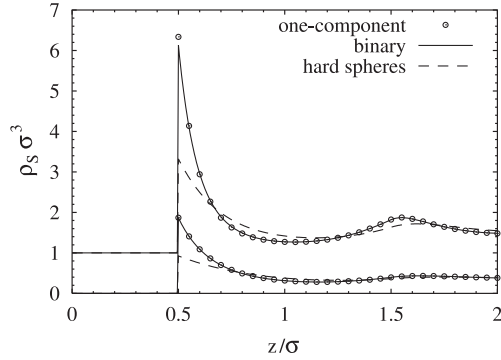


Fig. 2

Fig. 1 – Fluid-fluid demixing phase diagram for the rod-sphere mixture as a function of the sphere packing fraction, η , and scaled needle reservoir density, $\rho_N^r L^2 \sigma$, for size ratio $L/\sigma = 1$. The binodal (lines) and critical point (dots) from the binary and the effective one-component DFT are shown. Coexistence is along horizontal tie lines (not shown). The crosses mark statepoints where wall density profiles from both theories are compared in fig. 2. The arrow indicates a path along which wetting profiles are presented in fig. 3. The rectangle near the vertical axis indicates the region where the surface phase transitions near a hard wall are investigated in figs. 4 and 5.

Fig. 2 – Sphere density profiles, $\rho_S(z)\sigma^3$, at a hard wall as a function of the scaled distance, z/σ , from the wall for size ratio $L/\sigma = 1$ at two statepoints (marked by crosses in fig. 1): $\eta = 0.2$, $\rho_N^r L^2 \sigma = 5$ and $\eta = 0.3$, $\rho_N^r L^2 \sigma = 10$ (shifted upwards one unit for clarity). For comparison, the corresponding hard-sphere results (for the same values of η but $\rho_N^r = 0$) are displayed. Except for the region very near to contact with the wall ($z/\sigma \approx 0.5$) in the case of the higher packing fraction, the results from both theories are indistinguishable on the scale of the plot.

component treatment for the statepoint with higher densities. The good overall agreement for phase behavior and structure thus provides a solid basis for our subsequent interface study.

We first approach the gas branch of the fluid demixing binodal not too far from the critical point at $\rho_N^r \sigma L^2 = 16$ and increasing η , as indicated by the arrow in the phase diagram, fig. 1. A representative set of wall density profiles approaching coexistence is depicted in fig. 3 obtained from the one-component (upper panel) and binary (lower panel) treatments. Close to the wall, pronounced oscillations appear that can be attributed to packing effects of the spheres. For increasing z , the crossover to the low gas bulk density occurs via an intermediate plateau value of liquid-like density. The thickness of this region grows, and eventually diverges, upon approaching coexistence. The wall is wet completely by the colloidal liquid phase. The profiles from the one-component treatment possess a markedly thinner wetting film and a sharper interface of the liquid-gas part than those from the binary treatment. This is consistent with the difference in bulk phase diagrams. For the fixed value of ρ_N^r , the binary theory is relatively closer to its critical point, hence thicker films and broader liquid-gas interfaces are expected. We can, however, get similar wetting film thicknesses from the one-component treatment by going even closer to coexistence; an example of $\rho_S(z)$ is shown in fig. 3 (dashed line). Both theories consistently predict complete wetting, differences in the detailed structure can be fully understood from the differences in the respective bulk phase diagrams.

Having gained confidence into the one-component description, we use this computationally efficient approach to calculate the full surface phase diagram. As a first path we scan the phase diagram right at coexistence along the gas branch of the binodal by decreasing ρ_N^r (and

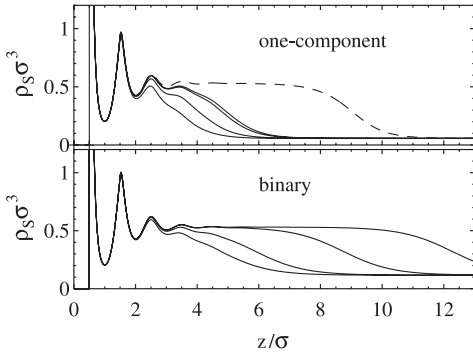


Fig. 3

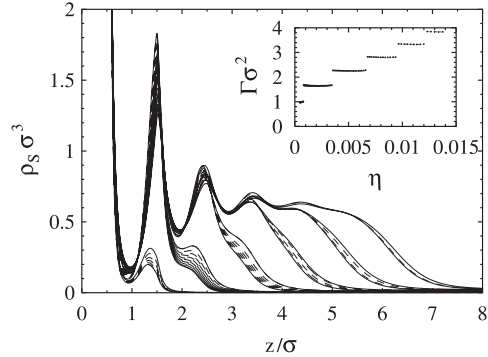


Fig. 4

Fig. 3 – Wetting density profiles, $\rho_S(z)\sigma^3$, as a function of the scaled distance from the wall, z/σ , for needle reservoir density $\rho_N^r L^2 \sigma = 16$ following the path marked in fig. 1 and obtained from the one-component (upper panel) and the binary (lower panel) treatment. The profiles are for $(\eta_{\text{coex}} - \eta)/\eta_{\text{coex}} = 0.01305, 0.004894, 0.001631, 0.001305$ (from left to right); coexistence is at $\eta_{\text{coex}} = 0.06130$ (binary), 0.02994 (one-component). The dashed line in the upper panel indicates the one-component result even closer to coexistence, $(\eta_{\text{coex}} - \eta)/\eta_{\text{coex}} = 5.77 \cdot 10^{-6}$.

Fig. 4 – Sequence of sphere density profiles, $\rho_S(z)\sigma^3$, as a function of the scaled distance from the wall, z/σ , obtained from the one-component treatment for statepoints at coexistence moving down the gas-branch of the fluid demixing binodal. Density profiles from left to right correspond to increasing η and decreasing $\rho_N^r L^2 \sigma$, spaced in steps of $\Delta \rho_N^r L^2 \sigma = 0.04$ (dashed lines). Five pronounced jumps occur, the corresponding density profiles at these layering transitions are indicated by solid lines. The inset shows the corresponding adsorption $\Gamma \sigma^2$ as a function of η .

accordingly increasing η). Our aim is to stay below the triple point, which is obtained from perturbation theory at $\rho_N^r \approx 25$ [3]. For high ρ_N^r the excess adsorption, $\Gamma = \int dz(\rho_S(z) - \rho_S(\infty))$, is finite at coexistence, *i.e.* the liquid wets the wall partially. Decreasing ρ_N^r continuously leads to several (five) jumps in the density profiles and correspondingly in Γ , see fig. 4. The sixth jump is that to a bulk liquid, *i.e.* the wetting point. Along our chosen path all layering transitions and the wetting transition are first order.

To reveal the full surface phase diagram we have covered the region of stability of the gas phase in the phase diagram on a fine grid. From anomalies in the density profiles, *i.e.* from jumps in Γ , the full surface phase diagram is constructed, see fig. 5 for the result. Due to our method of locating the interfacial transitions, their exact location is subject to some hysteresis effects. By calculating the adsorption along the reverse path, *i.e.* along the binodal from low ρ_N^r to high ρ_N^r , we could confirm that these effects are very small. We find that the five layering transitions all extend into the bulk gas region. Moving away from coexistence along such a layering line the jump in the adsorption decreases in magnitude and eventually ends in a critical point. The first layering transition is very pronounced, the subsequent transition lines decrease in length. The transition point on the binodal closest to the critical point is the wetting point; for rod densities below the corresponding value (and above the critical point), complete wetting occurs. We could not find the corresponding prewetting line where a transition from a thin to a thick line appears, and conclude that it is too small to be identified within our current numerical accuracy.

The whole pattern of surface phase transitions found from this description using pair potentials is very similar to that recently found in a related model colloid-polymer mixture taking

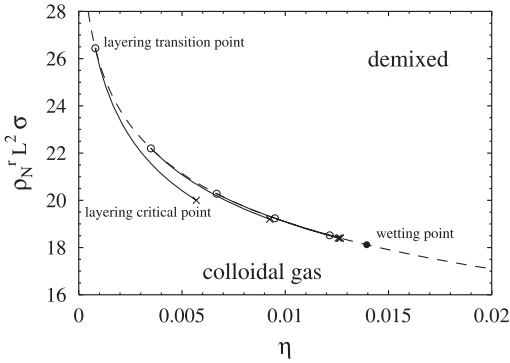


Fig. 5

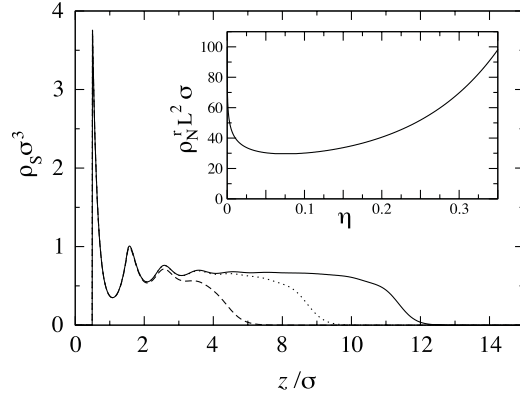


Fig. 6

Fig. 5 – Surface phase diagram of the rod-sphere mixture at a hard wall as a function of the sphere packing fraction, η , and scaled needle reservoir density, $\rho_N^r L^2 \sigma$, for size ratio $L/\sigma = 1$ obtained from the one-component theory. Shown are the bulk fluid demixing binodal (dashed line), layering transition points on the binodal (open circles), layering transition lines (solid lines), layering critical points (crosses), and wetting point (filled circle). The plot range corresponds to the rectangle in fig. 1.

Fig. 6 – Sphere density profiles $\rho_S(z)\sigma^3$ as a function of the distance z/σ from the wall for size ratio $L/\sigma = 5$, needle reservoir density $\rho_*^r = 100$ and increasing bulk colloid packing fraction $\eta = 1.04 \cdot 10^{-5}$ (dashed line), $1.06 \cdot 10^{-5}$ (dotted line) and $1.065 \cdot 10^{-5}$ (full line) obtained from the binary theory. Coexistence is at $\eta_{\text{coex}} = 1.077 \cdot 10^{-5}$. The inset shows the fluid demixing binodal as a function of η and needle reservoir density ρ_*^r for $L/\sigma = 5$.

into account all many-body interactions between colloids, *i.e.* treating the full binary mixture [14,15]. In that case, the inclusion of many-body terms is crucial; no layering transitions were found from a pair-wise treatment [14].

We believe that the occurrence of layering phase transitions is due to a subtle interplay between the relative strength of the particle-particle and the particle-wall attractions. Due to the particle geometries for the present case of rod depletants, the particle-wall attraction is relatively stronger than in the case of spherical (polymer) depletants. In that case a similar (relative) strengthening of the wall-particle attraction can happen due to the many-body terms. As a test for this hypothesis we have rescaled the wall-particle attraction, *i.e.* used $\lambda W_{\text{SW}}(z)$, $0 \leq \lambda \leq 1$, which artificially interpolates between the actual physical situation ($\lambda = 1$) and a (hypothetical) wall without depletion attraction ($\lambda = 0$). Indeed we find for $\lambda = 0.5$ complete wetting without any indications of layering transitions anywhere in the partial-wetting regime.

As a final investigation we consider a case of markedly longer rods: $L/\sigma = 5$. We expect many-body terms in the effective Hamiltonian to be important and that the effective one-component description with pair-wise interactions only will break down. In fact the phase diagram resulting from the one-component treatment is no longer comparable to the still rather accurate [3] binary treatment. From the binary DFT we find that thick films can be obtained even far away from the critical point, see fig. 6 for profiles close to the triple point at $\rho_N^r L^2 \sigma = 100$ [23]. Hence for observing thick films in experiment large L/σ are suitable.

In conclusion, we have investigated the adsorption properties of a colloidal mixture of rods and spheres at a hard wall. We find that for low rod densities the sphere liquid wets the wall completely upon approaching the fluid-fluid demixing binodal from the gas side. For high rod densities, above the wetting point, partial wetting occurs via a finite sequence of

layering phase transitions, where the adsorption jumps by finite increments. We argue that the crucial parameter for the occurrence of such layering transitions is the relative strength of wall-particle and particle-particle depletion interactions.

Colloidal mixtures of rods and spheres can be prepared so that they closely resemble the model system of hard spheres and needles [12] considered here. Therefore, our findings should be experimentally observable. In particular, it would be highly interesting to observe thick wetting films in the complete-wetting regime, *e.g.* with light [16] or confocal microscopy.

* * *

We thank R. EVANS for many inspiring discussions and R. VAN ROIJ and M. DIJKSTRA for valuable comments. The work of MS is part of the research program of FOM, that is financially supported by the Nederlandse Organisatie voor Wetenschappelijk Onderzoek (NWO).

REFERENCES

- [1] ADAMS M., DOGIC Z., KELLER S. L. and FRADEN S., *Nature (London)*, **393** (1998) 349.
- [2] VAN DER SCHOOT P., *J. Chem. Phys.*, **117** (2002) 3537.
- [3] BOLHUIS P. and FRENKEL D., *J. Chem. Phys.*, **101** (1994) 9869.
- [4] VLIAGENTHART G. A. and LEKKERKERKER H. N. W., *J. Chem. Phys.*, **111** (1999) 4153.
- [5] CHEN Y. L. and SCHWEIZER K. S., *J. Chem. Phys.*, **117** (2002) 1351; *Langmuir*, **18** (2002) 7354.
- [6] KOENDERINK G. H., VLIAGENTHART G. A., KLUIJTMANS S. G. J. M., VAN BLAADEREN A., PHILIPSE A. P. and LEKKERKERKER H. N. W., *Langmuir*, **15** (1999) 4693.
- [7] VLIAGENTHART G. A., Dissertation, Utrecht University (1999).
- [8] KOENDERINK G. H., AARTS D. G. A. L., DE VILLENEUVE V. W. A., PHILIPSE A. P., TUINIER R. and LEKKERKERKER H. N. W., *Biomacromolecules*, **4** (2003) 129.
- [9] YAMAN K., JEPPESEN C. and MARQUES C. M., *Europhys. Lett.*, **42** (1998) 221.
- [10] LIN K., CROCKER J. C., ZERI A. C. and YODH A. G., *Phys. Rev. Lett.*, **87** (2001) 088301.
- [11] LAU A. W. C., LIN K. H. and YODH A. G., *Phys. Rev. E*, **66** (2002) 020401.
- [12] HELDEN L., ROTH R., KOENDERINK G. H., LEIDERER P. and BECHINGER C., *Phys. Rev. Lett.*, **90** (2003) 048301.
- [13] ROTH R., *J. Phys. Condens. Matter*, **15** (2003) S277.
- [14] BRADER J. M., EVANS R., SCHMIDT M. and LÖWEN H., *J. Phys. Condens. Matter*, **14** (2002) L1.
- [15] DIJKSTRA M. and VAN ROIJ R., *Phys. Rev. Lett.*, **89** (2002) 208303.
- [16] AARTS D. G. A. L., VAN DER WIEL J. H. and LEKKERKERKER H. N. W., *J. Phys. Condens. Matter*, **15** (2003) S245.
- [17] WIJTING W. K., BESSELING N. A. M. and COHEN STUART M. A., unpublished.
- [18] See, *e.g.*, EVANS R., in *Fundamentals of Inhomogeneous Fluids*, edited by HENDERSON D. (Marcel Dekker, New York) 1992, p. 85.
- [19] SCHMIDT M., *Phys. Rev. E*, **63** (2001) 050201(R).
- [20] BRADER J. M., ESZTERMANN A. and SCHMIDT M., *Phys. Rev. E*, **66** (2002) 031401.
- [21] ROSENFELD Y., *Phys. Rev. Lett.*, **63** (1989) 980.
- [22] WEEKS J. D., CHANDLER D. and ANDERSEN H. C., *J. Chem. Phys.*, **54** (1971) 5237.
- [23] We take η_{coex} determined by the numerical minimization of the DFT; the result from the analytic free energy is $\eta_{\text{coex}} = 1.0598 \cdot 10^{-4}$.